Available online at www.sciencedirect.com
SCIENCE DIRECT®
International Journal of Heat and Mass Transfer 47 (2004) 4911–4927
International Journal of HEAT and MASS TRANSFER
www.elsevier.com/locate/ijhmt

Prandtl number dependence of unsteady natural convection along a vertical plate in a stably stratified fluid

Alan Shapiro *, Evgeni Fedorovich

School of Meteorology, University of Oklahoma, 100 East Boyd, Room 1310, Norman, OK 73019, USA

Received 30 September 2003

Abstract

The Prandtl number dependence of unsteady laminar natural convection along an infinite vertical plate in a thermally stratified fluid is investigated. Flows are induced by an impulsive (step) change in plate temperature and by a suddenly imposed plate heat flux. Analytical solutions of the viscous equations of motion and thermodynamic energy are obtained for Prandtl numbers near unity by the method of Laplace transforms and a regular perturbation expansion. The zeroth-, first- and second-order terms in the expansion are obtained for an impulsive change in plate temperature, while the zeroth- and first-order terms are obtained for a sudden application of a plate heat flux. The developing boundary layers are thicker, more vigorous, and more sensitive to the Prandtl number at smaller Prandtl numbers (<1) than at larger Prandtl numbers (>1). The analytical results are confirmed and extended with results from numerical simulations for Prandtl numbers strongly deviating from unity.

Keywords: Natural convection; Unsteady flow; Vertical plate; Stratified fluid; Prandtl number

1. Introduction

The unsteady natural convection flow of a viscous fluid along a vertical plate is a classical problem in fluid mechanics and heat transfer, with significance for a variety of engineering applications [1]. In the case where the plate is doubly-infinite (no leading edges), the Boussinesq equations of motion and thermodynamic energy reduce to one-dimensional forms, and the problem becomes amenable to analytical treatment. Solutions by the method of Laplace transforms have been obtained for a variety of plate boundary conditions [2–7], assuming the fluid is unstratified. These exact solutions provide rare analytical descriptions of transient natural convection flows and are potentially valuable as a means of validating numerical convection models.

The classical framework was recently extended by Park and Hyun [8], Park [9], and Shapiro and Fedorovich [10] (hereafter referred to as SF) to include thermal stratification. SF also made provision for pressure work for a perfect gas, a term that is neglected in the conventional Boussinesq approximation. This term can also be neglected in the SF theory by slightly modifying the stratification parameter; the description is then suitable for Boussinesq flow of liquids or gases. Park and Hyun [8], and Park [9] considered flow in the gap between two parallel plates, while SF considered flow in the semi-infinite domain bounded by a single plate. Steady-state solutions for these flows were obtained by Gill [11] and Elder [12].

With attention restricted to fluid of Prandtl number unity, SF obtained analytical solutions for the cases of impulsive (step) change in plate perturbation temperature, sudden application of a plate heat flux, and for arbitrary temporal variations in plate perturbation temperature or plate heat flux. Thermal stratification provided a negative feedback mechanism whereby rising fluid cooled relative to the environment, while subsiding

* Corresponding author. Tel.: +1-405-325-6097; fax: +1-405-325-7689.
E-mail address: ashapiro@ou.edu (A. Shapiro).

0017-9310/$ - see front matter © 2004 Elsevier Ltd. All rights reserved.
doi:10.1016/j.ijheatmasstransfer.2004.04.035

Nomenclature

c_p	specific heat at constant pressure
C	Fresnel cosine integral, $C(\chi) \equiv \int_0^\chi \cos(\pi\chi'^2/2)\,\mathrm{d}\chi'$
g	acceleration due to gravity
I_1, $I_{3/2}$	modified Bessel functions of first kind of orders 1 and 3/2, respectively
J_1, $J_{3/2}$	Bessel functions of first kind of orders 1 and 3/2, respectively
k	wavenumber
K	wavenumber separating oscillatory-decay modes from non-oscillatory-decay modes (defined in (64))
K^*	dominant boundary-layer wavenumber (defined in (65))
L^{-1}	inverse Laplace transform operator
p	pressure
p'	normalized pressure deviation from ambient value, $p' \equiv (p - p_\infty)/\rho_\mathrm{r}$
Pr	Prandtl number, $Pr \equiv v/\kappa$
Q_0	plate heat flux
s	Laplace transform parameter
t	time
T	temperature
T'	temperature perturbation, $T' \equiv T - T_\infty$
T'_0	temperature perturbation at plate
u_i	i'th component of velocity vector
w	vertical velocity
W	nondimensional vertical velocity (defined in (4) and (5))
x	plate-normal Cartesian coordinate
x_i	i'th component Cartesian coordinate ($x_1 = x, x_2 = y, x_3 = z$)
y	horizontal Cartesian coordinate in the plane of the plate
z	vertical (along-plate) Cartesian coordinate

Greek symbols

β	buoyancy parameter
γ	stratification parameter, $\gamma \equiv \mathrm{d}T_\infty/\mathrm{d}z$ (Boussinesq flow of liquids or gases), or $\gamma \equiv \mathrm{d}T_\infty/\mathrm{d}z + g/c_p$ (perfect gas, pressure work term retained)
δ	nondimensional steady-state boundary layer thickness
δ_{ij}	Kronecker delta tensor
ε	small parameter, $\varepsilon \equiv Pr - 1$
θ	nondimensional perturbation temperature (defined in (4) and (5))
κ	thermal diffusivity
v	kinematic viscosity
ξ	nondimensional distance perpendicular to plate (defined in (3))
ρ	density
τ	nondimensional time (defined in (3))
τ', τ''	dummy integration variables
ω	complex frequency (defined in (63))

Subscripts

$0, 1, 2, \ldots, n$	order of term in series expansion
i, j	tensor indices: $i = 1, 2, 3$; $j = 1, 2, 3$
pn	particular solution of n'th differential equation (21) in series expansion
r	reference value, a constant
s	steady state solution
t	transient solution
∞	ambient value of dependent variable as $x \to \infty$, a function of height

Superscripts

$\wedge$	Laplace-transformed variable
$-$	Fourier sine-transformed variable

fluid warmed relative to the environment. Provision for stratification allowed the solutions to approach steady-state conditions at large times, whereas if there is no stratification (classical solutions), the solutions grow without bound.

The present investigation extends the SF framework to fluids of arbitrary Prandtl number. First, analytical results are obtained in the form of a perturbation expansion for Prandtl numbers near unity. The zeroth-, first-, and second-order terms in the expansion are obtained for an impulsive change in plate temperature, while the zeroth- and first-order terms are obtained for a sudden application of a plate heat flux. A numerical model of convection is then introduced to solve the equations of motion and thermodynamic energy numerically. The numerical results confirm the analytical theory and extend the results to fluids with Prandtl numbers that differ significantly from unity. Finally, we develop a qualitative theory of the flow induced by an impulsive change in plate temperature valid for arbitrary Prandtl numbers.

The one-dimensional solutions described herein are valid for times prior to the arrival of disturbances originating at the leading edge, and prior to the onset of any flow instabilities. Although we have not yet explored the stability of these unsteady solutions, the stability of the steady state has been investigated in [13,14]. Flow stability was found to decrease with increasing plate temperature and increase with increasing stratification. In light of those studies and the laboratory experiments

in [15–17], the main interest in our solutions will likely be in cases where the stratification is large enough to delay or prevent flow instability.

2. Governing equations and perturbation expansion

The governing equations and nondimensionalization are discussed in SF, and will only be briefly summarized herein. Consider a Cartesian coordinate system in which x is the horizontal (plate-normal) coordinate and z is the vertical (plate-parallel) coordinate. The plate is located at $x = 0$, and fluid fills the semi-infinite domain $x > 0$. The fluid is quiescent until the imposition of a uniform thermal disturbance at the plate (temperature perturbation or heat flux) at times $t \geqslant 0$. The governing equations are the vertical equation of motion and thermodynamic energy equation,

$$\frac{\partial w}{\partial t} = g\frac{T'}{T_r} + \nu\frac{\partial^2 w}{\partial x^2}, \tag{1}$$

$$\frac{\partial T'}{\partial t} = -\gamma w + \kappa\frac{\partial^2 T'}{\partial x^2}. \tag{2}$$

Here $w(x,t)$ is the vertical velocity, $T'(x,t) \equiv T(x,z,t) - T_\infty(z)$ is the temperature perturbation (actual temperature T minus a linearly-varying ambient temperature $T_\infty(z)$), and $\gamma \equiv \mathrm{d}T_\infty/\mathrm{d}z + g/c_p$ is the stratification parameter. The flow scenario is illustrated schematically in Fig. 1.

The above form of γ is appropriate if we include temperature advection and pressure work in the thermodynamic energy equation, and consider a perfect gas. However, pressure work is often of minor importance, and is neglected in the Boussinesq approximation. If we neglect it in our work (by redefining γ as $\gamma \equiv \mathrm{d}T_\infty/\mathrm{d}z$), our theory then applies to Boussinesq flow of liquids and gases.

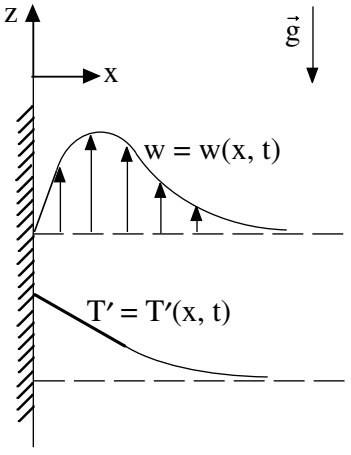

Fig. 1. One-dimensional (parallel) natural convection flow along an infinite vertical plate.

The independent variables x and t are nondimensionalized as

$$\xi \equiv x\frac{(g\gamma/T_r)^{1/4}}{\sqrt{\nu}}, \quad \tau \equiv t\sqrt{\frac{g\gamma}{T_r}}. \tag{3}$$

For flow induced by an impulsive change in plate perturbation temperature, $T'(0,t) = T'_0$, we nondimensionalize the dependent variables as

$$\theta \equiv \frac{T'}{T'_0}, \quad W \equiv \frac{w}{T'_0}\sqrt{\gamma T_r/g}, \tag{4}$$

while for flow induced by sudden application of a plate heat flux, $Q_0 = -\kappa\partial T'/\partial x(0,t)$, we use

$$\theta \equiv T'\frac{\kappa(g\gamma/T_r)^{1/4}}{Q_0\sqrt{\nu}}, \quad W \equiv w\frac{\kappa\gamma^{3/4}(T_r/g)^{1/4}}{Q_0\sqrt{\nu}}. \tag{5}$$

The nondimensional versions of (1) and (2) are

$$\frac{\partial W}{\partial \tau} = \theta + \frac{\partial^2 W}{\partial \xi^2}, \tag{6}$$

$$\frac{\partial \theta}{\partial \tau} = -W + \frac{1}{Pr}\frac{\partial^2 \theta}{\partial \xi^2}, \tag{7}$$

The nondimensional boundary conditions are

$$W(0,\tau) = 0 \quad \text{(no-slip)}, \tag{8}$$

$$W(\infty,\tau) = 0, \quad \theta(\infty,\tau) = 0 \quad \text{(disturbance vanishes far from plate)} \tag{9}$$

and either

$$\theta(0,\tau) = 1 \quad \text{(constant plate perturbation temperature)} \tag{10a}$$

or

$$\frac{\partial \theta}{\partial \xi}(0,\tau) = -1 \quad \text{(constant plate heat flux)}. \tag{10b}$$

The steady-state solutions (valid for $\tau \to \infty$) presented in [11,14] and SF, are $\theta_s(\xi) = A\cos\times(\xi Pr^{1/4}/\sqrt{2})\exp(-\xi Pr^{1/4}/\sqrt{2})$, $W_s(\xi) = B\sin(\xi Pr^{1/4}/\sqrt{2})\exp(-\xi Pr^{1/4}/\sqrt{2})$, where $A = 1$, $B = Pr^{-1/2}$ for step-change in plate temperature, and $A = \sqrt{2}Pr^{-1/4}$, $B = \sqrt{2}Pr^{-3/4}$ for suddenly applied plate heat flux. The peak nondimensional vertical velocity occurs at a distance $\delta = \pi\sqrt{2}Pr^{-1/4}/4$ from the plate, and has the value $W_s(\delta) = B\exp(-\pi/4)/\sqrt{2}$. Although the boundary layer thickness δ increases with decreasing Pr, the dependence is weak (small exponent) except for $Pr \ll 1$. The Reynolds numbers based on the dimensional values of δ and $W_s(\delta)$ are $Re \simeq 0.358T'_0(g\kappa^3/\nu^5 T_r\gamma^3)^{1/4}$ for a step-change in plate temperature, and $Re \simeq 0.506Q_0/\nu\gamma$ for a sudden application of a plate heat flux. In either case Re

increases with decreasing viscosity and decreasing stratification parameter.

At early times, when the temperature gradient near the plate is large and the vertical velocity is small, the dominant thermodynamic process is conduction, and the first term on the right hand side of (7) (accounting for temperature advection and pressure work) is negligible. Since the equation set without this term describes the classical (unstratified) scenario, the analytical solutions obtained in [2–7] also apply to the early stages of convection in the stratified environment.

With ε defined as the deviation of the Prandtl number from unity, $\varepsilon = Pr - 1$, (6) and (7) become

$$\frac{\partial W}{\partial \tau} = \theta + \frac{\partial^2 W}{\partial \xi^2}, \tag{11}$$

$$(1+\varepsilon)\frac{\partial \theta}{\partial \tau} = -(1+\varepsilon)W + \frac{\partial^2 \theta}{\partial \xi^2}. \tag{12}$$

Multiplying (11) and (12) by $e^{-s\tau}$ and integrating from $\tau = 0$ to $\tau = \infty$ yields a pair of coupled ordinary differential equations,

$$s\widehat{W} = \hat{\theta} + \frac{d^2\widehat{W}}{d\xi^2}, \tag{13}$$

$$(1+\varepsilon)s\hat{\theta} = -(1+\varepsilon)\widehat{W} + \frac{d^2\hat{\theta}}{d\xi^2}, \tag{14}$$

for the Laplace-transformed variables $\hat{\theta} \equiv \int_0^\infty \theta e^{-s\tau} d\tau$ and $\widehat{W} \equiv \int_0^\infty W e^{-s\tau} d\tau$.

Using (14) to eliminate $\widehat{W}$ in favor of $\hat{\theta}$ in (13), we obtain a single fourth-order ordinary differential equation for $\hat{\theta}$,

$$\frac{d^4\hat{\theta}}{d\xi^4} - s(2+\varepsilon)\frac{d^2\hat{\theta}}{d\xi^2} + (1+\varepsilon)(s^2+1)\hat{\theta} = 0. \tag{15}$$

It can readily be shown that $\widehat{W}$ satisfies an equation of the same form as (15).

With attention restricted to Prandtl numbers near unity, ε is a small parameter and we seek solutions of (15) for $\hat{\theta}$ (and for $\widehat{W}$) in the form of regular perturbation expansions in ε [18]:

$$\begin{aligned} \hat{\theta} &= \hat{\theta}_0 + \varepsilon\hat{\theta}_1 + \varepsilon^2\hat{\theta}_2 + \cdots = \sum_{n=0}^{\infty} \varepsilon^n \hat{\theta}_n, \\ \widehat{W} &= \widehat{W}_0 + \varepsilon\widehat{W}_1 + \varepsilon^2\widehat{W}_2 + \cdots = \sum_{n=0}^{\infty} \varepsilon^n \widehat{W}_n. \end{aligned} \tag{16}$$

As we will see, the differential equations and boundary conditions for $\hat{\theta}_n$ and $\widehat{W}_n$ are independent of ε. Accordingly, after computing them (once), they can be applied in (16) to obtain the solutions for $\hat{\theta}$ and $\widehat{W}$ for any Prandtl number near unity. The solutions for the original variables θ and W then follow by taking the inverse Laplace transform L^{-1} of (16), and using the linearity of the L^{-1} operator,

$$\theta = \sum_{n=0}^{\infty} \varepsilon^n \theta_n, \quad W = \sum_{n=0}^{\infty} \varepsilon^n W_n, \tag{17}$$

where $\theta_n \equiv L^{-1}(\hat{\theta}_n)$ and $W_n \equiv L^{-1}(\widehat{W}_n)$.

3. Analytical solutions

In this section we obtain the analytical solutions for a step-change in plate temperature through the second-order terms, and for sudden application of a plate heat flux through the first-order terms. Readers not interested in the mathematical details can skip to Section 4.

3.1. General form of the transformed variables

Applying (16) in (15), and collecting terms in common powers of ε, we obtain a sequence of differential equations for the $\hat{\theta}_n$,

$$\begin{aligned} &\frac{d^4\hat{\theta}_n}{d\xi^4} - 2s\frac{d^2\hat{\theta}_n}{d\xi^2} + (s^2+1)\hat{\theta}_n \\ &\quad = \begin{cases} 0, & n = 0, \\ s\dfrac{d^2\hat{\theta}_{n-1}}{d\xi^2} - (s^2+1)\hat{\theta}_{n-1}, & n \geqslant 1. \end{cases} \end{aligned} \tag{18}$$

Since the disturbance vanishes far from the plate, $\hat{\theta}_0$ is of the form

$$\hat{\theta}_0 = a_0 \exp(-\xi\sqrt{s+i}) + b_0 \exp(-\xi\sqrt{s-i}), \tag{19}$$

while the higher order functions $\hat{\theta}_n$ ($n \geqslant 1$) are of the form

$$\hat{\theta}_n = a_n \exp(-\xi\sqrt{s+i}) + b_n \exp(-\xi\sqrt{s-i}) + \hat{\theta}_{pn}, \tag{20}$$

where $\hat{\theta}_{pn}$ is any particular solution of

$$\begin{aligned} &\frac{d^4\hat{\theta}_{pn}}{d\xi^4} - 2s\frac{d^2\hat{\theta}_{pn}}{d\xi^2} + (s^2+1)\hat{\theta}_{pn} \\ &\quad = s\frac{d^2\hat{\theta}_{n-1}}{d\xi^2} - (s^2+1)\hat{\theta}_{n-1}, \quad n \geqslant 1. \end{aligned} \tag{21}$$

Setting $n = 1$ in (21), and making use of (19) for $\hat{\theta}_0$, we see that $\hat{\theta}_{p1}$ must satisfy

$$\begin{aligned} &\frac{d^4\hat{\theta}_{p1}}{d\xi^4} - 2s\frac{d^2\hat{\theta}_{p1}}{d\xi^2} + (s^2+1)\hat{\theta}_{p1} \\ &\quad = ia_0(s+i)\exp(-\xi\sqrt{s+i}) - ib_0(s-i) \\ &\qquad \times \exp(-\xi\sqrt{s-i}). \end{aligned} \tag{22}$$

It can readily be verified that a particular solution of (22) is of the form $\hat{\theta}_{p1} = A\xi\exp(-\xi\sqrt{s+i}) +$

$B\xi\exp(-\xi\sqrt{s-i})$, where $A=-a_0\sqrt{s+i}/4$, and $B=-b_0\sqrt{s-i}/4$. Thus, $\hat{\theta}_1$ is of the form

$$\hat{\theta}_1=\left(a_1-\frac{a_0}{4}\sqrt{s+i}\xi\right)\exp(-\xi\sqrt{s+i})+\left(b_1-\frac{b_0}{4}\sqrt{s-i}\xi\right)\exp(-\xi\sqrt{s-i}). \tag{23}$$

Proceeding to (22) with $n=2$ and making use of (23) for $\hat{\theta}_1$, we see that $\hat{\theta}_{p2}$ must satisfy

$$\frac{\mathrm{d}^4\hat{\theta}_{p2}}{\mathrm{d}\xi^4}-2s\frac{\mathrm{d}^2\hat{\theta}_{p2}}{\mathrm{d}\xi^2}+(s^2+1)\hat{\theta}_{p2}=\left[\left(\frac{s}{2}a_0+ia_1\right)(s+i)-\frac{i}{4}a_0(s+i)^{3/2}\xi\right]\times\exp(-\xi\sqrt{s+i})+\left[\left(\frac{s}{2}b_0-ib_1\right)(s-i)+\frac{i}{4}b_0(s-i)^{3/2}\xi\right]\times\exp(-\xi\sqrt{s-i}). \tag{24}$$

A particular solution of (24) is $\hat{\theta}_{p2}=(C\xi+D\xi^2)\exp(-\xi\sqrt{s+i})+(E\xi+F\xi^2)\exp(-\xi\sqrt{s-i})$, where $D=a_0(s+i)/32$, $F=b_0(s-i)/32$, $C=[(3+2si)a_0/32-a_1/4]\sqrt{s+i}$, and $E=[(3-2si)b_0/32-b_1/4]\sqrt{s-i}$. Thus we can write $\hat{\theta}_2$ as

$$\hat{\theta}_2=\left\{a_2+\left[(3+2si)\frac{a_0}{32}-\frac{a_1}{4}\right]\sqrt{s+i}\xi+\frac{a_0}{32}(s+i)\xi^2\right\}\times\exp(-\xi\sqrt{s+i})+\left\{b_2+\left[(3-2si)\frac{b_0}{32}-\frac{b_1}{4}\right]\sqrt{s-i}\xi+\frac{b_0}{32}(s-i)\xi^2\right\}\exp(-\xi\sqrt{s-i}). \tag{25}$$

Since the differential equation for $\widehat{W}$ is identical to (15), and the disturbance vanishes far from the plate, (19), (23), and (25) also describe the generic forms of $\widehat{W}_0$, $\widehat{W}_1$, and $\widehat{W}_2$, respectively.

3.2. Boundary conditions

For an impulsive change in plate temperature, transform the plate conditions (10a) and (8) into $\hat{\theta}(0)=1/s$ and $\widehat{W}(0)=0$, and apply them in (14) and (13), obtaining $\mathrm{d}^2\hat{\theta}/\mathrm{d}\xi^2(0)=1+\varepsilon$ and $\mathrm{d}^2\widehat{W}/\mathrm{d}\xi^2(0)=-1/s$. Expanding these with (16) yields the temperature functions at the plate as

$$\hat{\theta}_n(0)=\begin{cases}\frac{1}{s}, & n=0,\\ 0, & n\geqslant 1,\end{cases} \tag{26}$$

$$\frac{\mathrm{d}^2\hat{\theta}_n}{\mathrm{d}\xi^2}(0)=\begin{cases}1, & n=0,1,\\ 0, & n\geqslant 2,\end{cases} \tag{27}$$

and the velocity functions at the plate as

$$\widehat{W}_n(0)=0,\quad n\geqslant 0, \tag{28}$$

$$\frac{\mathrm{d}^2\widehat{W}_n}{\mathrm{d}\xi^2}(0)=\begin{cases}-\frac{1}{s}, & n=0,\\ 0, & n\geqslant 1.\end{cases} \tag{29}$$

For a suddenly imposed heat flux, apply the transforms of (10b) and (8) ($\mathrm{d}\hat{\theta}/\mathrm{d}\xi(0)=-1/s$ and $\widehat{W}(0)=0$) in (14) and in the ξ-derivative of (13), obtaining $(1+\varepsilon)s\hat{\theta}(0)=\mathrm{d}^2\hat{\theta}/\mathrm{d}\xi^2(0)$ and $s\,\mathrm{d}\widehat{W}/\mathrm{d}\xi(0)=-1/s+\mathrm{d}^3\widehat{W}/\mathrm{d}\xi^3(0)$. In view of (16), the temperature functions at the plate become

$$\frac{\mathrm{d}\hat{\theta}_n}{\mathrm{d}\xi}(0)=\begin{cases}-\frac{1}{s}, & n=0,\\ 0, & n\geqslant 1,\end{cases} \tag{30}$$

$$\frac{\mathrm{d}^2\hat{\theta}_n}{\mathrm{d}\xi^2}(0)-s\hat{\theta}_n(0)=\begin{cases}0, & n=0,\\ s\hat{\theta}_{n-1}(0), & n\geqslant 1,\end{cases} \tag{31}$$

and the velocity functions at the plate become

$$\widehat{W}_n(0)=0,\quad n\geqslant 0, \tag{32}$$

$$\frac{\mathrm{d}^3\widehat{W}_n}{\mathrm{d}\xi^3}(0)-s\frac{\mathrm{d}\widehat{W}_n}{\mathrm{d}\xi}(0)=\begin{cases}\frac{1}{s}, & n=0,\\ 0, & n\geqslant 1.\end{cases} \tag{33}$$

3.3. Solution for impulsive (step) change of plate temperature

Applying (26) and (27) in (19) for $n=0$ yields $a_0=b_0=1/(2s)$, and so

$$\hat{\theta}_0=\frac{1}{2s}\exp(-\xi\sqrt{s+i})+\frac{1}{2s}\exp(-\xi\sqrt{s-i}). \tag{34}$$

Applying (26) and (27) in (23) for $n=1$ yields $a_1=-i/4$, $b_1=i/4$, and so

$$\hat{\theta}_1=-\frac{i}{4}\left[\exp(-\xi\sqrt{s+i})-\exp(-\xi\sqrt{s-i})\right]-\frac{1}{8}\xi\left[\frac{1}{s}\sqrt{s+i}\exp(-\xi\sqrt{s+i})+\frac{1}{s}\sqrt{s-i}\exp(-\xi\sqrt{s-i})\right]. \tag{35}$$

Applying (26) and (27) in (25) for $n=2$ yields $a_2=i/8, b_2=-i/8$, and so

$$\hat{\theta}_2=\frac{i}{8}\left[\exp(-\xi\sqrt{s+i})-\exp(-\xi\sqrt{s-i})\right]+\frac{3}{64}\xi\left[\frac{1}{s}\sqrt{s+i}\exp(-\xi\sqrt{s+i})+\frac{1}{s}\sqrt{s-i}\exp(-\xi\sqrt{s-i})\right]+\frac{3i}{32}\xi\left[\sqrt{s+i}\exp(-\xi\sqrt{s+i})-\sqrt{s-i}\times\exp(-\xi\sqrt{s-i})\right]+\frac{1}{64}\xi^2\left[\frac{1}{s}(s+i)\times\exp(-\xi\sqrt{s+i})+\frac{1}{s}(s-i)\exp(-\xi\sqrt{s-i})\right]. \tag{36}$$

Similarly, application of (28) and (29) in (19), (23), and (25) (the generic forms for both the transformed temperature functions and the transformed velocity functions) yields

$$\widehat{W}_0 = \frac{i}{2s}\exp(-\xi\sqrt{s+i}) - \frac{i}{2s}\exp(-\xi\sqrt{s-i}), \tag{37}$$

$$\begin{aligned}\widehat{W}_1 = {} & -\frac{i}{4}\left[\frac{1}{s}\exp(-\xi\sqrt{s+i}) - \frac{1}{s}\exp(-\xi\sqrt{s-i})\right] \\ & -\frac{i}{8}\xi\left[\frac{1}{s}\sqrt{s+i}\exp(-\xi\sqrt{s+i}) \right. \\ & \left. -\frac{1}{s}\sqrt{s-i}\exp(-\xi\sqrt{s-i})\right],\end{aligned} \tag{38}$$

$$\begin{aligned}\widehat{W}_2 = {} & \frac{1}{16}\left[\exp(-\xi\sqrt{s+i}) + \exp(-\xi\sqrt{s-i})\right] \\ & +\frac{i}{16}\left[(s+i)\exp(-\xi\sqrt{s+i}) - (s-i)\right. \\ & \left.\times\exp(-\xi\sqrt{s-i})\right] \\ & +\frac{3i}{16}\left[\frac{1}{s}\exp(-\xi\sqrt{s+i}) - \frac{1}{s}\exp(-\xi\sqrt{s-i})\right] \\ & +\frac{7i}{64}\xi\left[\frac{1}{s}\sqrt{s+i}\exp(-\xi\sqrt{s+i}) - \frac{1}{s}\sqrt{s-i}\right. \\ & \left.\times\exp(-\xi\sqrt{s-i})\right] - \frac{1}{32}\xi\left[\sqrt{s+i}\right. \\ & \left.\times\exp(-\xi\sqrt{s+i}) + \sqrt{s-i}\right. \\ & \left.\times\exp(-\xi\sqrt{s-i})\right] + \frac{i}{64}\xi^2\left[\frac{1}{s}(s+i)\right. \\ & \left.\times\exp(-\xi\sqrt{s+i}) - \frac{1}{s}(s-i)\exp(-\xi\sqrt{s-i})\right].\end{aligned} \tag{39}$$

The inverse transforms $\theta_n \equiv L^{-1}(\hat{\theta}_n)$ and $W_n \equiv L^{-1}(\widehat{W}_n)$ for $n = 0, 1$ and 2 are readily evaluated using the tabulated transforms in Appendix A together with the integration theorem, $L^{-1}[g(s)/s] = \int_0^\tau G(\tau')\,\mathrm{d}\tau'$, where $G(\tau) = L^{-1}g(s)$. The solutions can be expressed as

$$\theta_0 = \frac{\xi}{2\sqrt{\pi}}\int_0^\tau \frac{\cos\tau'}{\tau'^{3/2}}\exp\left(-\frac{\xi^2}{4\tau'}\right)\mathrm{d}\tau', \tag{40}$$

$$\begin{aligned}\theta_1 = {} & -\frac{\xi\sin\tau}{4\sqrt{\pi}\tau^{3/2}}\exp\left(-\frac{\xi^2}{4\tau}\right) - \frac{\xi}{16\sqrt{\pi}} \\ & \times\int_0^\tau \frac{(\xi^2-2\tau')\cos\tau'}{\tau'^{5/2}}\exp\left(-\frac{\xi^2}{4\tau'}\right)\mathrm{d}\tau',\end{aligned} \tag{41}$$

$$\begin{aligned}\theta_2 = {} & \frac{\xi(3\xi^2+2\tau)\sin\tau}{64\sqrt{\pi}\tau^{5/2}}\exp\left(-\frac{\xi^2}{4\tau}\right) + \frac{\xi}{256\sqrt{\pi}} \\ & \times\int_0^\tau \frac{(\xi^4-12\tau'^2)\cos\tau'}{\tau'^{7/2}}\exp\left(-\frac{\xi^2}{4\tau'}\right)\mathrm{d}\tau',\end{aligned} \tag{42}$$

$$W_0 = \frac{\xi}{2\sqrt{\pi}}\int_0^\tau \frac{\sin\tau'}{\tau'^{3/2}}\exp\left(-\frac{\xi^2}{4\tau'}\right)\mathrm{d}\tau', \tag{43}$$

$$W_1 = -\frac{\xi}{16\sqrt{\pi}}\int_0^\tau \frac{(2\tau'+\xi^2)\sin\tau'}{\tau'^{5/2}}\exp\left(-\frac{\xi^2}{4\tau'}\right)\mathrm{d}\tau', \tag{44}$$

$$\begin{aligned}W_2 = {} & \frac{\xi(6\tau-\xi^2)(\tau\cos\tau-\sin\tau)}{64\sqrt{\pi}\tau^{7/2}}\exp\left(-\frac{\xi^2}{4\tau}\right) \\ & +\frac{\xi}{256\sqrt{\pi}}\int_0^\tau \frac{(\xi^4+8\xi^2\tau'+20\tau'^2)\sin\tau'}{\tau'^{7/2}} \\ & \times\exp\left(-\frac{\xi^2}{4\tau'}\right)\mathrm{d}\tau',\end{aligned} \tag{45}$$

where τ' is a dummy integration variable. The integrals in (40)–(45) were evaluated with the trapezoidal formula using a time step of $\Delta\tau = 0.001$. Such a high temporal resolution was required for an accurate evaluation of the integrals near the plate because of the singular nature of the integrands as $\xi \to 0$. As shown in SF, the singularity in (40) compensates for the vanishing of ξ in front of the integral, and allows the recovery of the desired boundary condition $\theta_0 \to 1$ as $\xi \to 0$. It can be shown that all of the other functions in (41)–(45) vanish at the plate.

3.4. Solution for sudden application of plate heat flux

Applying (30) and (31) in (19) for $n = 0$ yields $a_0\sqrt{s+i} + b_0\sqrt{s-i} = 1/s$ and $a_0 = b_0$, from which follow $a_0 = b_0 = -i(\sqrt{s+i} - \sqrt{s-i})/(2s)$. We thus obtain

$$\begin{aligned}\hat{\theta}_0 = {} & -\frac{i}{2}(\sqrt{s+i} - \sqrt{s-i})\left[\frac{1}{s}\exp(-\xi\sqrt{s+i})\right. \\ & \left.+\frac{1}{s}\exp(-\xi\sqrt{s-i})\right].\end{aligned} \tag{46}$$

Applying (30) and (31) in (23) for $n = 1$ yields $a_1\sqrt{s+i} + b_1\sqrt{s-i} = -1/(4s)$ and $a_1 - b_1 = -(\sqrt{s+i} - \sqrt{s-i})/2$, from which follow

$$\begin{aligned}a_1 &= \frac{i}{8s}(\sqrt{s+i} - \sqrt{s-i}) + \frac{i}{4}\sqrt{s-i}(\sqrt{s+i} - \sqrt{s-i})^2, \\ b_1 &= \frac{i}{8s}(\sqrt{s+i} - \sqrt{s-i}) - \frac{i}{4}\sqrt{s+i}(\sqrt{s+i} - \sqrt{s-i})^2.\end{aligned} \tag{47}$$

It is convenient to rewrite (47) as

$$\begin{aligned}a_1 = {} & \frac{i}{8s}(\sqrt{s+i} - \sqrt{s-i}) - \frac{i}{4}(\sqrt{s+i} - \sqrt{s-i})^3 \\ & +\frac{i}{4}\sqrt{s+i}(\sqrt{s+i} - \sqrt{s-i})^2, \\ b_1 = {} & \frac{i}{8s}(\sqrt{s+i} - \sqrt{s-i}) - \frac{i}{4}(\sqrt{s+i} - \sqrt{s-i})^3 \\ & -\frac{i}{4}\sqrt{s-i}(\sqrt{s+i} - \sqrt{s-i})^2.\end{aligned} \tag{48}$$

in order to obtain the first order transformed temperature function as

$$\hat{\theta}_1 = \frac{i}{8}(\sqrt{s+i}-\sqrt{s-i})\left[\frac{1}{s}\exp(-\xi\sqrt{s+i}) + \frac{1}{s}\exp(-\xi\sqrt{s-i})\right] - \frac{i}{4}(\sqrt{s+i} - \sqrt{s-i})^3\left[\exp(-\xi\sqrt{s+i}) + \exp(-\xi\sqrt{s-i})\right] + \frac{i}{4}(\sqrt{s+i}-\sqrt{s-i})^2\left[\sqrt{s+i}\exp(-\xi\sqrt{s+i}) - \sqrt{s-i}\exp(-\xi\sqrt{s-i})\right] + \frac{i}{8}\xi(\sqrt{s+i} - \sqrt{s-i})\left[\frac{1}{s}\sqrt{s+i}\exp(-\xi\sqrt{s+i}) + \frac{1}{s}\sqrt{s-i}\exp(-\xi\sqrt{s-i})\right]. \quad (49)$$

The evaluation of $\widehat{\theta}_2$ and $\widehat{W}_2$ for this case is based on the same techniques, but is exceedingly tedious and was not completed.

Application of (32) and (33) in (19) and (23), written in terms of $\widehat{W}_0$ and $\widehat{W}_1$, respectively, followed by some lengthy algebraic manipulations yields the transformed velocity functions as

$$\widehat{W}_0 = \frac{1}{2}(\sqrt{s+i}-\sqrt{s-i})\left[\frac{1}{s}\exp(-\xi\sqrt{s+i}) - \frac{1}{s}\exp(-\xi\sqrt{s-i})\right], \quad (50)$$

$$\widehat{W}_1 = -\frac{3}{8}(\sqrt{s+i}-\sqrt{s-i})\left[\frac{1}{s}\exp(-\xi\sqrt{s+i}) - \frac{1}{s}\exp(-\xi\sqrt{s-i})\right] + \frac{1}{8}(\sqrt{s+i} - \sqrt{s-i})^3\left[\exp(-\xi\sqrt{s+i}) - \exp(-\xi\sqrt{s-i})\right] - \frac{1}{8}(\sqrt{s+i} - \sqrt{s-i})\xi\left[\frac{1}{s}\sqrt{s+i}\exp(-\xi\sqrt{s+i}) - \frac{1}{s}\sqrt{s-i}\exp(-\xi\sqrt{s-i})\right]. \quad (51)$$

To evaluate the inverse transforms of these functions we use the convolution theorem, $L^{-1}[f(s)g(s)] = \int_0^\tau G(\tau')F(\tau-\tau')\,\mathrm{d}\tau'$, where $G(\tau) = L^{-1}g(s)$, and $F(\tau) = L^{-1}f(s)$, and the integration theorem in conjunction with standard results presented in Appendix A. We obtain

$$\theta_0 = \frac{\xi}{2\pi}\int_0^\tau \frac{\sin(\tau-\tau')}{(\tau-\tau')^{3/2}}\int_0^{\tau'}\frac{\cos\tau''}{\tau''^{3/2}}\exp\left(-\frac{\xi^2}{4\tau''}\right)\mathrm{d}\tau''\,\mathrm{d}\tau', \quad (52)$$

$$\theta_1 = \frac{3\xi}{2\pi}\int_0^\tau \frac{[(\tau-\tau')\cos(\tau-\tau') - \sin(\tau-\tau')]}{(\tau-\tau')^{5/2}} \times \frac{\cos\tau'}{\tau'^{3/2}}\exp\left(-\frac{\xi^2}{4\tau'}\right)\mathrm{d}\tau' - \frac{1}{4\sqrt{\pi}}\int_0^\tau \frac{J_1(\tau-\tau')}{\tau-\tau'} \times \frac{(\xi^2-2\tau')\sin\tau'}{\tau'^{5/2}}\exp\left(-\frac{\xi^2}{4\tau'}\right)\mathrm{d}\tau' - \frac{\xi^3}{16\pi}\int_0^\tau \frac{\sin(\tau-\tau')}{(\tau-\tau')^{3/2}}\int_0^{\tau'}\frac{\cos\tau''}{\tau''^{5/2}} \times \exp\left(-\frac{\xi^2}{4\tau''}\right)\mathrm{d}\tau''\,\mathrm{d}\tau', \quad (53)$$

$$W_0 = \frac{\xi}{2\pi}\int_0^\tau \frac{\sin(\tau-\tau')}{(\tau-\tau')^{3/2}}\int_0^{\tau'}\frac{\sin\tau''}{\tau''^{3/2}}\exp\left(-\frac{\xi^2}{4\tau''}\right)\mathrm{d}\tau''\,\mathrm{d}\tau', \quad (54)$$

$$W_1 = \frac{3\xi}{4\pi}\int_0^\tau \frac{[(\tau-\tau')\cos(\tau-\tau') - \sin(\tau-\tau')]}{(\tau-\tau')^{5/2}} \times \frac{\sin\tau'}{\tau'^{3/2}}\exp\left(-\frac{\xi^2}{4\tau'}\right)\mathrm{d}\tau' - \frac{\xi}{4\pi} \times \int_0^\tau \frac{\sin(\tau-\tau')}{(\tau-\tau')^{3/2}}\int_0^{\tau'}\frac{\sin\tau''}{\tau''^{3/2}}\exp\left(-\frac{\xi^2}{4\tau''}\right)\mathrm{d}\tau''\,\mathrm{d}\tau' - \frac{\xi^3}{16\pi}\int_0^\tau \frac{\sin(\tau-\tau')}{(\tau-\tau')^{3/2}}\int_0^{\tau'}\frac{\sin\tau''}{\tau''^{5/2}} \times \exp\left(-\frac{\xi^2}{4\tau''}\right)\mathrm{d}\tau''\,\mathrm{d}\tau', \quad (55)$$

where τ' and τ'' are dummy integration variables.

As shown in SF, the formula for the zeroth-order function θ_0 simplifies at the plate to $\theta_0(0,\tau) = -\frac{2\sin\tau}{\sqrt{\pi\tau}} + 2^{3/2}C(\sqrt{2\tau/\pi})$, where $C(\chi) \equiv \int_0^\chi \cos(\pi\chi'^2/2)\,\mathrm{d}\chi'$ is a Fresnel cosine integral. Unfortunately, formula (53) for the first-order function θ_1 does not enjoy a similar simplification. However, since the normal component of the gradient of θ_1 is zero [Eq. (30) with $n = 1$], the distribution of θ_1 along the plate can readily be determined by extrapolating the solution from the first interior grid point to the plate.

The integrals in (52)–(55) were evaluated with the trapezoidal formula using a time step of $\Delta\tau = 0.001$. The Bessel function of first kind of order one J_1 appearing in (53) was evaluated with the first 20 terms of its ascending series representation [20], a sufficiently accurate representation for the times under consideration ($\tau \leqslant 10$).

4. Numerical simulation

The analytical solutions of the previous section are valid for Prandtl numbers near unity. To explore the limits of validity of these analytical solutions and to extend our investigation to a wider range of Prandtl numbers, we turn to numerical simulations. The

numerical procedures adopted herein are based on methods described in [21,22] applied in direct simulation mode.

Consider the (dimensional) Boussinesq forms of the equations of motion, thermodynamic energy, and mass conservation,

$$\frac{\partial u_i}{\partial t} + u_j \frac{\partial u_i}{\partial x_j} = -\frac{\partial p'}{\partial x_i} + \beta T' \delta_{i3} + \nu \frac{\partial^2 u_i}{\partial x_j^2}, \tag{56}$$

$$\frac{\partial T'}{\partial t} + u_j \frac{\partial T'}{\partial x_j} = -\gamma u_3 + \kappa \frac{\partial^2 T'}{\partial x_j^2}, \tag{57}$$

$$\frac{\partial u_i}{\partial x_i} = 0, \tag{58}$$

where $p' \equiv (p - p_\infty)/\rho_r$ is the normalized pressure deviation from its hydrostatic value, u_i $(i = 1, 2, 3)$ are the components of the velocity vector along the Cartesian coordinates x_i $(x_1 = x, x_2 = y, x_3 = z)$, δ_{ij} is the Kronecker delta tensor, and the Einstein summation convention for repeated indices is employed. Application of (58) in the equation resulting from taking the divergence of (56) yields a diagnostic equation for p',

$$\frac{\partial^2 p'}{\partial x_i^2} = -\frac{\partial}{\partial x_i}\left(u_j \frac{\partial u_i}{\partial x_j}\right) + \beta \frac{\partial T'}{\partial x_3}. \tag{59}$$

Although (56)–(59) apply to both laminar and turbulent regimes of convection, the present study is restricted to the laminar regime. The values of the plate thermal forcings (temperature perturbation or heat flux) and the physical parameters of the problem $(\beta, \gamma, \nu, \kappa)$ used for the simulations reported herein were such that the flow regime was laminar.

The governing equations were discretized on a staggered Cartesian grid in a rectangular domain stretched along the plate-normal (x) direction. The equations for the prognostic variables (u, v, w, T') were integrated over time with the leapfrog scheme, with an Asselin time filter used to prevent solution decoupling. The spatial derivatives were approximated with second-order finite-difference expressions. The Poisson equation (59) was solved at each time step with a Fast Fourier Transform technique over the y–z planes (vertical planes parallel to the plate), and a tridiagonal factorization method in the plate-normal direction. No-slip and impermeability conditions were applied on the velocity components at the plate. Values of p' at the plate were calculated from the truncated version of the third $(i = 3)$ equation of motion. At the opposite (large x) end of the computational domain, the normal gradients of all prognostic variables were set to zero. Periodic boundary conditions were imposed for all computed variables on the four x–y and x–z computational boundaries of the domain. The output velocity and temperature perturbation values were averaged over the y–z planes. However, as long as the flow remained laminar (which was the case for all results reported herein), variations of these quantities in the y–z planes were negligible. To facilitate comparisons with the analytical results, the output variables were nondimensionalized as in (3)–(5).

5. Analytical and numerical results

5.1. Code validation: results for $Pr = 1$

To validate the numerical code, we revisited the case of $Pr = 1$ (the subject of SF). This was the only case for which our analytical solutions were exact within the Boussinesq framework. Differences between the analytical and numerical solutions of θ and W were found to be nearly imperceptible at all times for both the impulsive change of plate temperature and the suddenly applied heat flux. A sample cross-section illustrating the

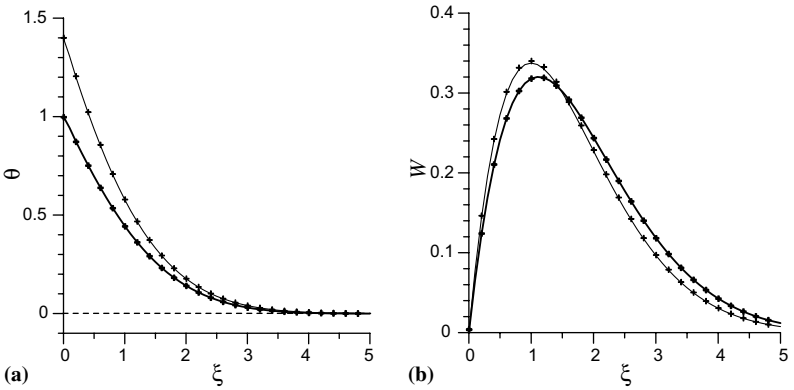

Fig. 2. Cross-sections of (a) θ and (b) W at $\tau = 2$ for $Pr = 1$. Bold solid lines indicate analytical solutions for impulsive change in plate temperature. Thin solid lines indicate analytical solutions for suddenly applied heat flux. Crosses indicate numerical simulation results.

nearly perfect agreement is depicted in Fig. 2 for $\tau = 2$. This diagram suggests that the numerical code is error free and that the numerical procedures are adequate to simulate the laminar flows under investigation. We now examine the details of the distributions of θ and W for a variety of Prandtl numbers.

5.2. Impulsive (step) change of plate temperature

Contour plots of the velocity and temperature functions $\theta_0, \theta_1, \theta_2, W_0, W_1$, and W_2 as functions of ξ and τ are presented in Fig. 3. The zeroth-order functions θ_0 and W_0 (which correspond to the exact solution for $Pr = 1$) have a boundary-layer character and approach steady state conditions through a temporally decaying oscillation. The zeroth-order temperature function θ_0 reverses sign on the periphery of the boundary layer, in a region roughly centered on $\xi = 2.5$. In the case of a hot plate, conduction spreads the heat outward from the plate, inducing a rising current of fluid adjacent to the plate. The viscous drag of this updraft on the environment forces the ascent and cooling of stably stratified fluid, resulting in a zone of cool fluid on the periphery of the updraft. A cross-section of these flow variables at $\tau = 2$ was shown in Fig. 2.

The patterns of the first-order functions W_1 and θ_1 are similar to (but slightly broader than) the patterns of the respective zeroth-order functions, W_0 and θ_0, while the patterns of the second-order functions W_2 and θ_2 are, in turn, similar to (but slightly broader than) the patterns of the first-order functions. The successive broadening of these functions is especially apparent in the locations of the zero-value isolines. We also note that the first-order functions are generally out of phase with the zeroth-order functions, while the second-order functions are generally in phase with the zeroth-order functions. However, since the first-order terms contribute to the overall solution through their product with ε, namely εW_1 and $\varepsilon\theta_1$, these terms make in-phase contributions to the solution (same phase as the zeroth-order functions) for $Pr < 1(\varepsilon < 0)$, but out-of-phase contributions for $Pr > 1(\varepsilon > 0)$. Moreover, since the second-order terms contribute to the overall solution through $\varepsilon^2\theta_2$ and $\varepsilon^2 W_2$ (which have the same signs as θ_2 and W_2 respectively), these terms always make in-phase contributions. Thus, for Prandtl numbers decreasing in value beneath unity, the zeroth-, first- and second-order functions are largely in phase, and tend to make the boundary layer thicker and more vigorous. In contrast, for Prandtl numbers larger than unity, the first-order terms counter the zeroth- and second-order terms, and result in a weaker boundary-layer flow.

Contour plots of the second-order approximate solutions for θ and W (sum of zeroth-, first- and second-order terms, $\theta \simeq \theta_0 + \varepsilon\theta_1 + \varepsilon^2\theta_2, W \simeq W_0 + \varepsilon W_1 + \varepsilon^2 W_2$) are presented in Fig. 4 for $Pr = 0.71(\varepsilon = -0.29)$, the Prandtl number for dry air at a temperature of 30°C at atmospheric pressure [23]. Cross-sections of these second-order approximate solutions at $\tau = 2$ are presented in Fig. 5. Also shown in Fig. 5 are the first-order approximate solutions, $\theta \simeq \theta_0 + \varepsilon\theta_1, W \simeq W_0 + \varepsilon W_1$, the zeroth-order approximate solutions, $\theta \simeq \theta_0, W \simeq W_0$, and the numerical solution. The differences between the second-order approximate solution and the numerical solution are nearly imperceptible throughout the cross-section. In the region of the peak vertical velocity, the first-order approximate solution falls a few percent short of the numerical solution, while the zeroth-order approximate solution falls nearly 20% short of the numerical solution.

Next consider cross-sections of the analytical and numerical solutions at $\tau = 2$ for the cases of $Pr = 0.5$ in Fig. 6(a)–(b) and $Pr = 1.5$ in Fig. 6(c)–(d). Even though the Prandtl numbers for these cases are no longer very close to unity, the second-order approximate solution is still quite close to the numerical solution (discrepancies of only a few percent of the numerical solution at the location of the peak vertical velocity). These cross-sections together with the previous cross-sections of Figs. (2) and (4) for $Pr = 1.0$ and 0.71 show the increase in peak boundary-layer velocity and boundary-layer thickness as the Prandtl number decreases. The relative magnitudes of the sequence of zeroth-, first- and second-order approximate solutions for θ and W indicate the in-phase contributions of the zeroth-, first- and second-order functions for $Pr < 1$, and the out-of-phase contribution of the first-order function with respect to the zeroth- and second-order functions for $Pr > 1$.

Lastly, consider the numerically simulated flow corresponding to a Prandtl number so much larger than unity that the analytical solutions would not be expected to be useful. Depicted in Fig. 7 are the flow variables obtained from a numerical simulation for $Pr = 7.1(\varepsilon = 6.1)$, the Prandtl number for pure water at a temperature of 20 °C at atmospheric pressure [23]. The peak vertical velocity and boundary layer thickness are greatly reduced from their corresponding values in the lower Prandtl number flows. The amplitude of the temporally-decaying wave-like part of the flow is also noticeably reduced from that of the lower Prandtl number flows.

5.3. Sudden application of plate heat flux

Contour plots of the zeroth- and first-order functions θ_0, θ_1, W_0, and W_1 as functions of ξ and τ are presented in Fig. 8 for the case of a suddenly applied heat flux (as noted in Section 3.4, the derivation of the second-order functions was not completed). As in the case of the impulsively changed plate temperature, the first-order functions are largely out of phase with the zeroth-order

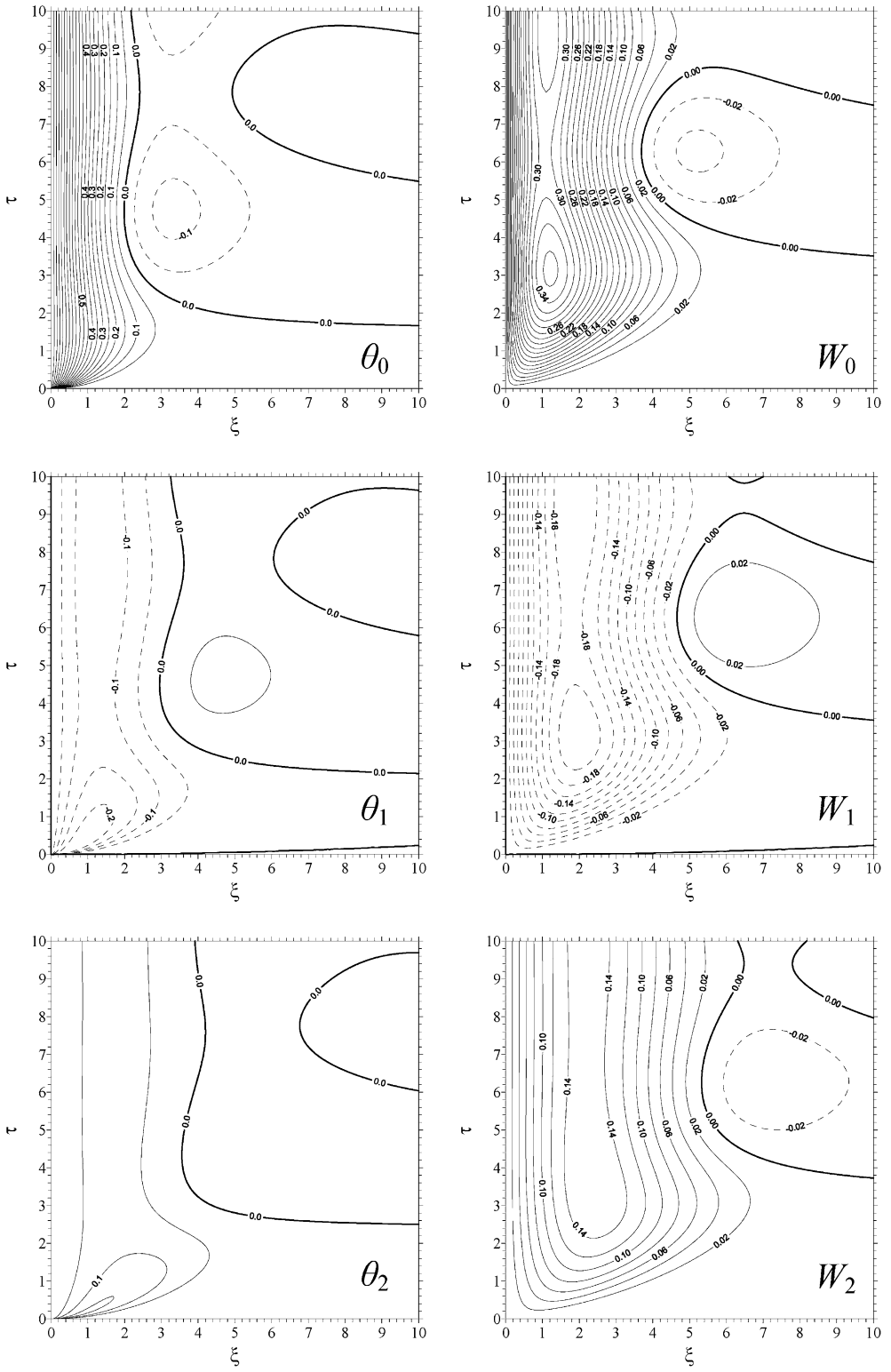

Fig. 3. Contour plots of zeroth-, first-, and second-order temperature functions (left-hand panels) and velocity functions (right-hand panels) for case of impulsive change in plate temperature. Contour intervals are 0.05 for temperature functions and 0.02 for velocity functions. Negative contours are dashed.

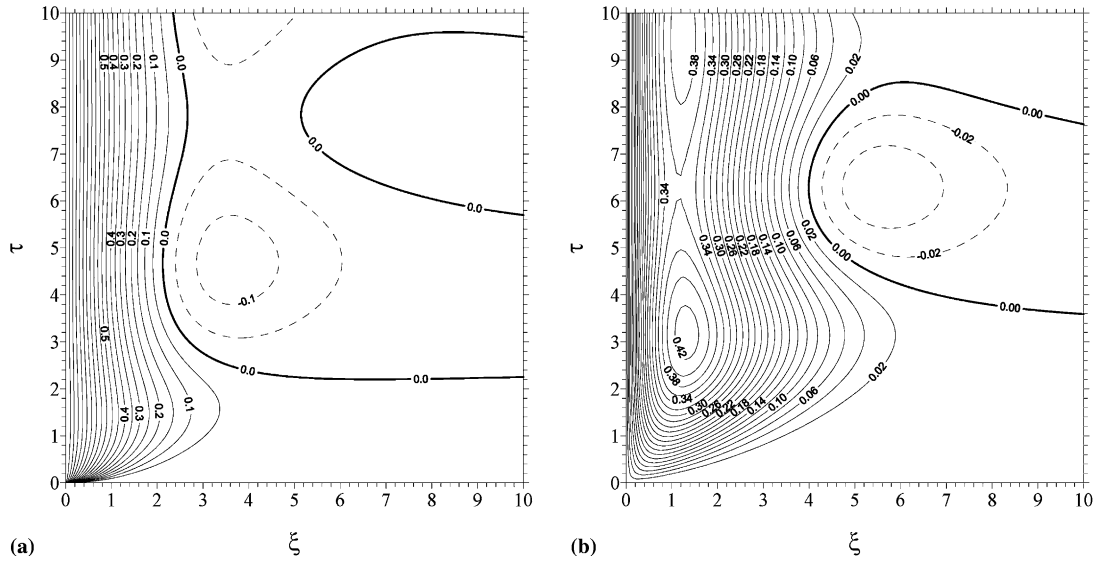

Fig. 4. Contour plots of second-order approximate solutions for case of impulsive change in plate temperature with $Pr = 0.71$: (a) $\theta \simeq \theta_0 + \varepsilon\theta_1 + \varepsilon^2\theta_2$ and (b) $W \simeq W_0 + \varepsilon W_1 + \varepsilon^2 W_2$. Contour intervals and labeling are as in Fig. 3.

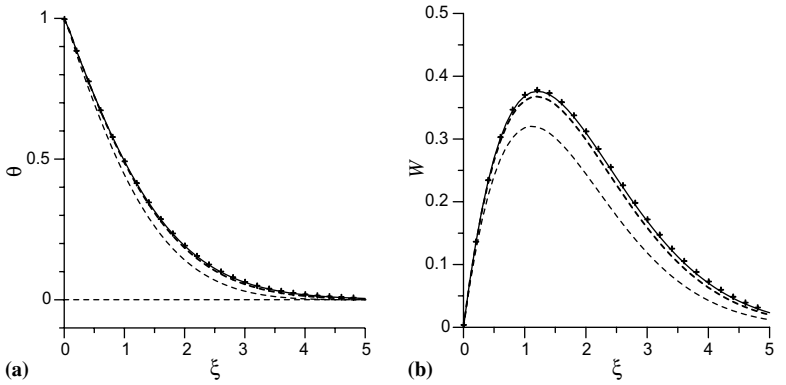

Fig. 5. Cross-sections of (a) θ and (b) W at $\tau = 2$ for case of impulsive change in plate temperature with $Pr = 0.71$. Bold dashed lines indicate zeroth-order approximate solutions, $\theta \simeq \theta_0$ and $W \simeq W_0$. Thin dashed lines indicate first-order approximate solutions, $\theta \simeq \theta_0 + \varepsilon\theta_1$ and $W \simeq W_0 + \varepsilon W_1$. Solid lines indicate second-order approximate solutions $\theta \simeq \theta_0 + \varepsilon\theta_1 + \varepsilon^2\theta_2$ and $W \simeq W_0 + \varepsilon W_1 + \varepsilon^2 W_2$. Crosses indicate numerical simulation results.

functions. Since the first-order functions contribute to the overall solution through their product with $\varepsilon(\varepsilon W_1$ and $\varepsilon\theta_1)$, these terms again make in-phase contributions to the solution (same phase as zeroth-order functions) for $Pr < 1(\varepsilon < 0)$, and out-of-phase contributions for $Pr > 1(\varepsilon > 0)$. Contour plots of the first-order approximate solutions $\theta \simeq \theta_0 + \varepsilon\theta_1$ and $W \simeq W_0 + \varepsilon W_1$ are presented in Fig. 9 for $Pr = 0.71(\varepsilon = -0.29)$. The flow patterns are qualitatively similar to those in the case of the impulsively changed plate temperature (Fig. 4). Cross-sections of this first-order approximate solution, the zeroth-order approximate solutions, $\theta \simeq \theta_0, W \simeq W_0$ and the numerical solution at $\tau = 2$ are presented in Fig. 10. The first-order approximate solution for W falls approximately 10% short of the corresponding numerical solution in the zone of peak vertical velocity, while the zeroth-order approximate solution falls short by approximately 30%. Cross-sections of the flow variables at $\tau = 2$ for $Pr = 0.5$ and 1.5 are presented in Fig. 11. A comparison of Figs. 11 and 6 shows that the discrepancies between these approximate solutions and the numerical solutions are larger in the suddenly applied heat flux case than in the case of an impulsive change in plate temperature.

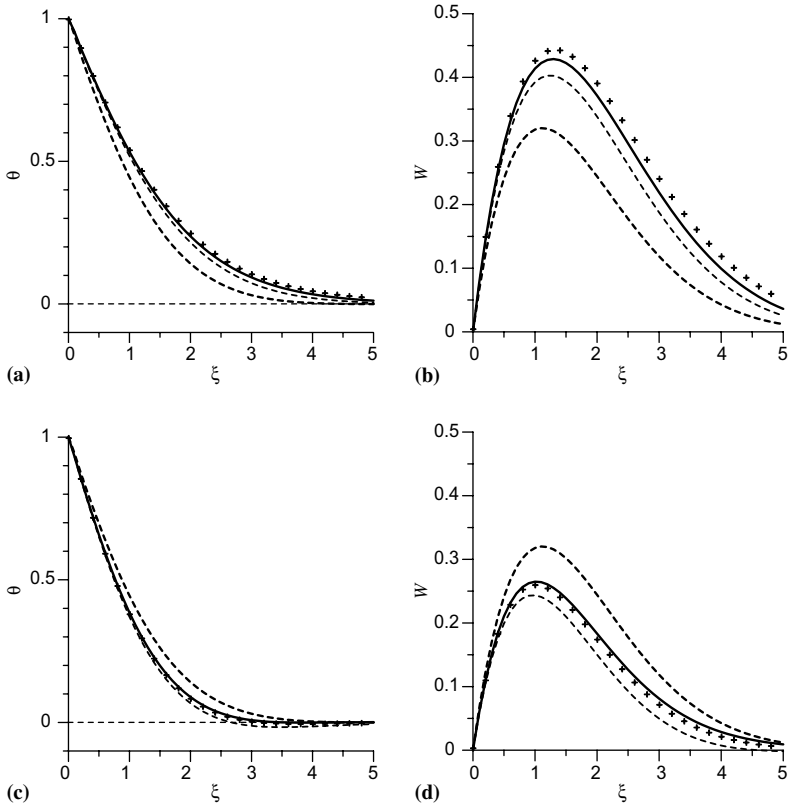

Fig. 6. As in Fig. 5 but for $Pr = 0.5$ [panels (a) and (b)] and $Pr = 1.5$ [panels (c) and (d)].

6. Qualitative behavior of the solution for arbitrary Prandtl number

The preceding solutions were characterized by an abrupt onset of convective flow adjacent to the plate followed by strongly or weakly oscillatory approaches to steady-state conditions. In this section we provide a brief qualitative discussion of the transient part of the solution for arbitrary Prandtl number. Attention is restricted to the case of an impulsive change in plate temperature.

We first decompose W and Θ into their steady-state and transient components, $W(\xi,\tau) = W_s(\xi) + W_t(\xi,\tau)$ and $\Theta(\xi,\tau) = \Theta_s(\xi) + \Theta_t(\xi,\tau)$, where W_s and Θ_s were described in Section 2. Substituting these forms into (6) and (7), we find that the transient components W_t and Θ_t satisfy partial differential equations identical to (6) and (7) subject to homogeneous boundary conditions. Multiplying those equations by $\sin k\xi$, and integrating from $\xi = 0$ to $\xi = \infty$, we obtain a pair of ordinary differential equations for the Fourier sine-transformed variables $\overline{W}(k,\tau) \equiv \int_0^\infty W_t \sin k\xi \, d\xi$ and $\overline{\Theta}(k,\tau) \equiv \int_0^\infty \Theta_t \sin k\xi \, d\xi$:

$$\frac{d\overline{W}}{d\tau} = \bar{\theta} - k^2\overline{W}, \tag{60}$$

$$\frac{d\bar{\theta}}{d\tau} = -\overline{W} - \frac{k^2}{Pr}\bar{\theta}. \tag{61}$$

Using (60) to eliminate $\bar{\theta}$ in favor of $\overline{W}$ in (61), we obtain

$$\frac{d^2\overline{W}}{d\tau^2} + k^2\left(1 + \frac{1}{Pr}\right)\frac{d\overline{W}}{d\tau} + \left(1 + \frac{k^4}{Pr}\right)\overline{W} = 0. \tag{62}$$

Eq. (62) admits solutions of the form $\overline{W} \sim e^{\omega\tau}$ provided ω satisfies $\omega^2 + k^2(1 + 1/Pr)\omega + 1 + k^4/Pr = 0$, that is

$$\omega = \frac{k^2}{2}\left(1 + \frac{1}{Pr}\right)\left[-1 \pm \sqrt{1 - 4\frac{1/k^4 + 1/Pr}{(1 + 1/Pr)^2}}\right]. \tag{63}$$

It can readily be shown that the real part of (63) is always negative, so all modes undergo a temporal decay. It can also be shown that the quantity under the radical sign in (63) vanishes for the wavenumber $k = K$ defined by

$$K \equiv \frac{\sqrt{2}}{\sqrt{|1 - 1/Pr|}}. \tag{64}$$

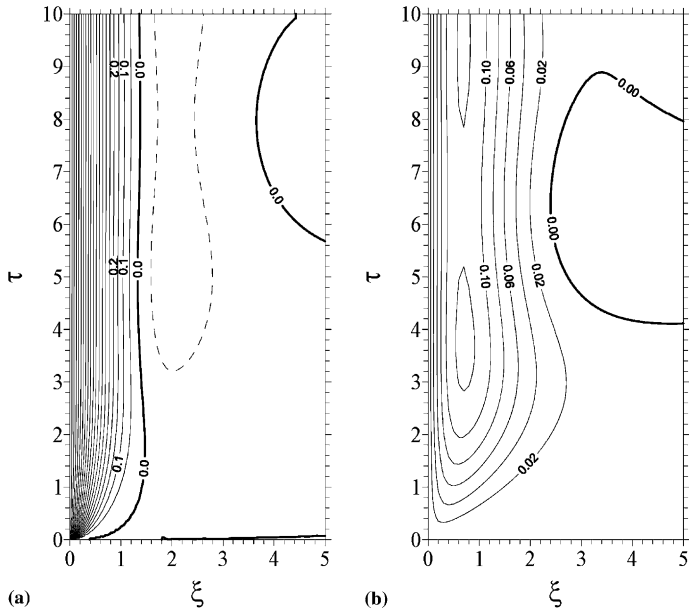

Fig. 7. Contour plots of (a) θ and (b) W from numerically simulated case of impulsive change in plate temperature with $Pr = 7.1$. Contour intervals and labeling are as in Fig. 3.

For small wavenumbers $k < K$, the quantity under the radical sign is negative, so ω is complex. These small wavenumbers are associated with oscillatory-decay modes. For large wavenumbers $k > K$, the quantity under the radical sign is positive and less than one, so ω is a negative real number (for both positive and negative solution branches). These wavenumbers are associated with non-oscillatory-decay modes. We note that for $Pr = 1, K$ is infinite and all modes are oscillatory-decay modes.

To determine whether the gross behavior of a flow corresponding to a particular Prandtl number is of oscillatory-decay type or non-oscillatory-decay type, we must check whether the dominant wavenumber of that flow is greater than or less than K. Toward that end, we introduce a reference wavenumber K^* based on the steady-state boundary layer thickness δ. The results in Section 5.2 suggest that the unsteady boundary layer thickness should be well-approximated by the steady-state boundary layer thickness for times after the initial burst (onset) of convection along the plate. Since W_s rises from zero at the plate to its maximum value at $\xi = \delta$ (shown in Section 2 to be $\delta = \pi\sqrt{2}Pr^{-1/4}/4$), we can interpret δ as the dominant quarter-wavelength of the flow. So $K^* = 2\pi/(4\delta)$, or

$$K^* = \sqrt{2}Pr^{1/4}. \tag{65}$$

This same formula would have resulted from a definition of K^* as the sine-transform-weighted mean of k,

$$K^* \equiv \frac{\int_0^\infty k\overline{W}_s(k)\,dk}{\int_0^\infty \overline{W}_s(k)\,dk} = \sqrt{2}Pr^{1/4}, \tag{66}$$

where $\overline{W}_s \equiv \int_0^\infty W_s \sin k\xi\,d\xi$, though the demonstration is lengthy and not given here.

The curves $K = K(Pr)$ and $K^* = K^*(Pr)$ are presented in Fig. 12. For Prandtl numbers near unity, $K^* < K$ and the gross behavior is of oscillatory-decay type. For large Prandtl numbers (e.g., $Pr = 7.1$), $K^* > K$ and the gross behavior is of non-oscillatory-decay type. These results are consistent with our finding in Section 5.2 that the solution for $Pr = 7.1$ was "less wavy" than the solutions for Prandtl numbers near unity.

7. Conclusions

This study extends the theory developed in SF for unsteady laminar natural convection along an infinite vertical plate in a thermally stratified fluid. The analytical solutions in that study were valid for a Prandtl number of unity. In the present investigation, approximate analytical solutions are obtained for Prandtl numbers near unity by the method of Laplace transforms and a regular perturbation expansion. The zeroth-, first- and second-order terms in the expansion are obtained for an impulsive change in plate temperature, while the zeroth- and first-order terms are obtained for a sudden application of a plate heat flux. The (exact) analytical solutions for $Pr = 1$ are used to benchmark a

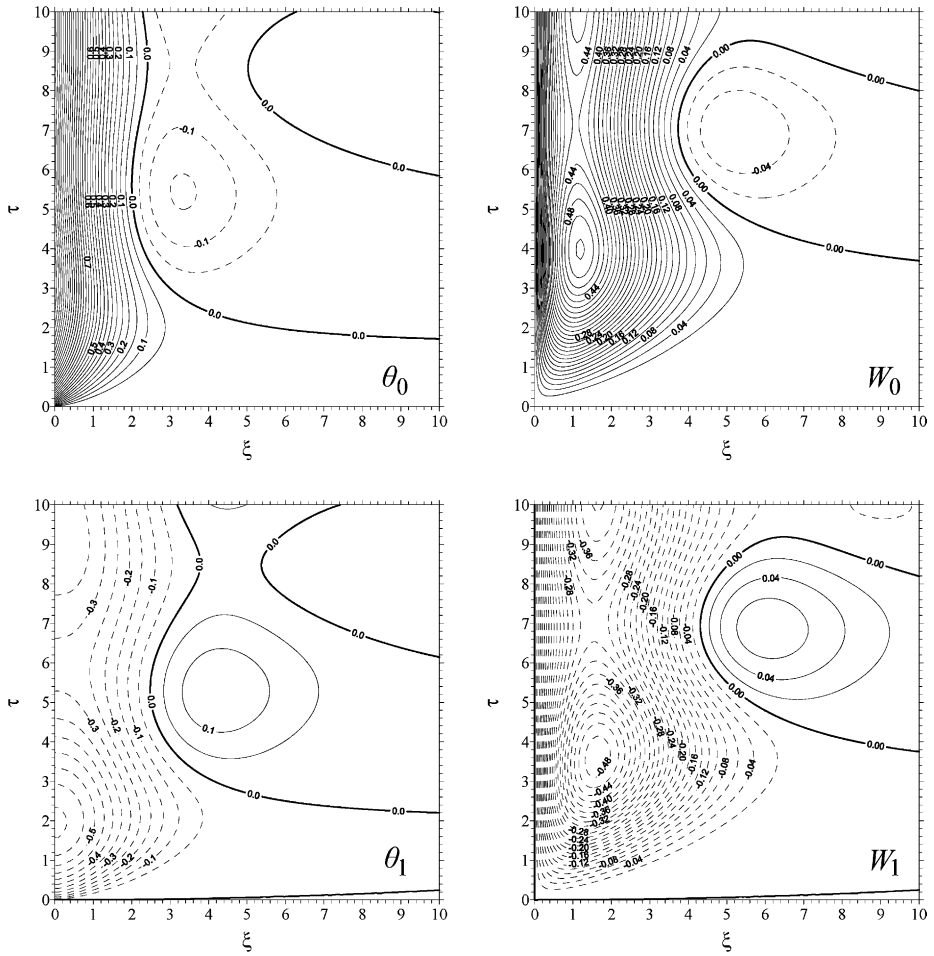

Fig. 8. Contour plots of zeroth- and first-order temperature functions (left-hand panels) and velocity functions (right-hand panels) for case of suddenly applied heat flux. Contour intervals and labeling are as in Fig. 3.

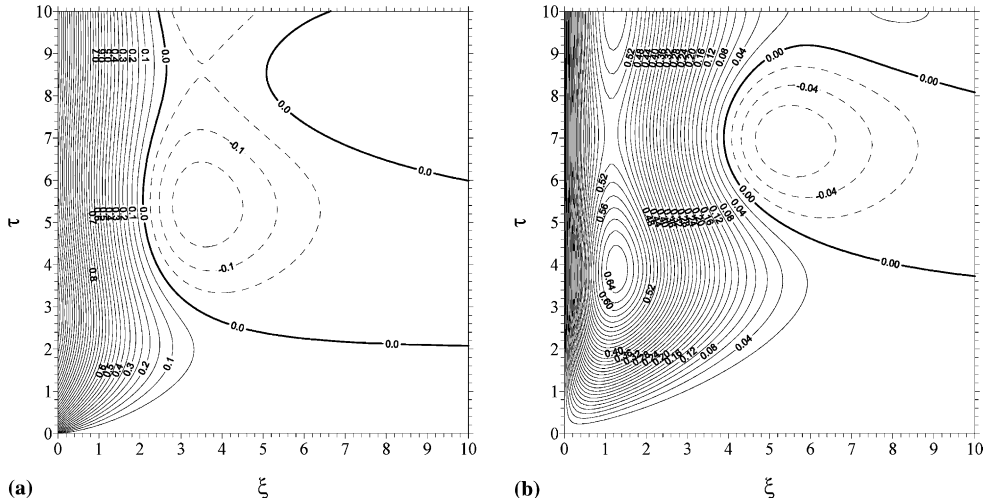

Fig. 9. Contour plots of first-order approximate solutions for case of suddenly applied heat flux with $Pr = 0.71$: (a) $\theta \simeq \theta_0 + \varepsilon\theta_1$ and (b) $W \simeq W_0 + \varepsilon W_1$. Contour intervals and labeling are as in Fig. 3.

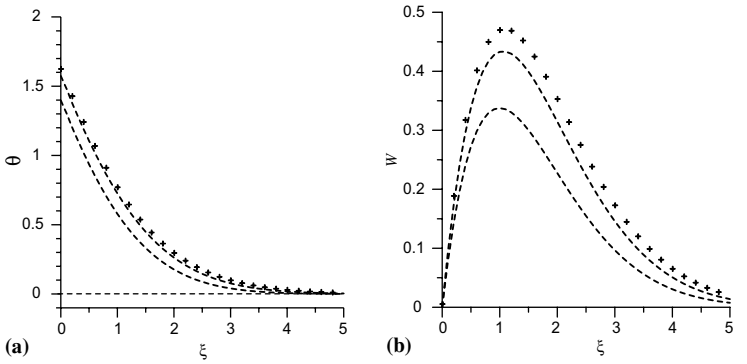

Fig. 10. Cross-sections of (a) θ and (b) W at $\tau = 2$ for case of suddenly applied heat flux with $Pr = 0.71$. Bold dashed lines indicate zeroth-order approximate solutions $\theta \simeq \theta_0$ and $W \simeq W_0$. Thin dashed lines indicate first-order approximate solutions $\theta \simeq \theta_0 + \varepsilon\theta_1$ and $W \simeq W_0 + \varepsilon W_1$. Crosses indicate numerical simulation results.

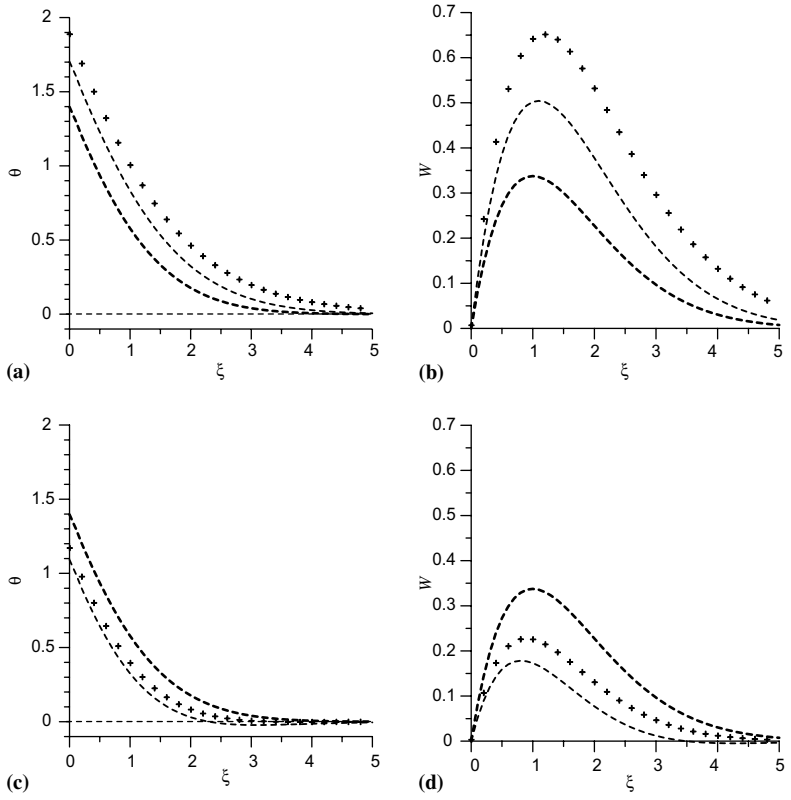

Fig. 11. As in Fig. 10 but for $Pr = 0.5$ [panels (a) and (b)] and $Pr = 1.5$ [panels (c) and (d)].

numerical model of convection which is then used to obtain numerical solutions for a variety of Prandtl numbers. In this manner, the accuracy of the analytical descriptions is explored for Prandtl numbers ranging between 0.5 and 1.5, including $Pr = 0.71$, the value for dry air at a temperature of 30 °C at atmospheric pressure. The second-order approximate solution for the case of the impulsive change in plate temperature yields a remarkably accurate flow description for Prandtl numbers in this range. A numerical simulation is also obtained for $Pr = 7.1$, the Prandtl number for pure water at a temperature of 20 °C at atmospheric pressure.

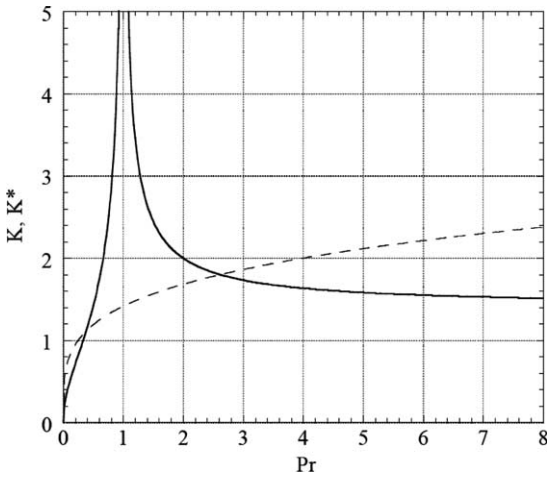

Fig. 12. Regime diagram for flow due to an impulsively changed plate temperature. Solid curves depict $K = K(Pr)$, the boundary in wavenumber space between oscillatory-decay modes ($k < K$) and non-oscillatory-decay modes ($k > K$). Dashed curve depicts $K^* = K^*(Pr)$, a reference wavenumber based on boundary-layer thickness.

The developing boundary layers in the investigated flow cases are found to be thicker, more vigorous and more sensitive to the Prandtl number at smaller Prandtl numbers (<1) than at larger Prandtl numbers (>1).

We also present a qualitative theory of flow behavior for arbitrary Prandtl number for the case of an impulsive change in plate temperature. The analysis considers the Fourier sine-transformed equations of motion, and examines the temporal behavior of each mode in wavenumber space as a function of Prandtl number. The analysis shows that the gross behavior of flows with Prandtl numbers near unity is of oscillatory-decay type, while the gross behavior of flows with large Prandtl numbers is of non-oscillatory-decay type.

It should be borne in mind, however, that all analytical and numerical results reported herein are valid for the laminar regime. Flow instabilities, transition to turbulence, and the structure of the resulting turbulent solutions will be examined in future studies.

Appendix A

The inverse transformations that led to the solutions in Sections 3.3 and 3.4 were obtained by applying the integration and convolution theorems to the results collected in this appendix. We have drawn on an extensive table of transforms (Roberts and Kaufman [19], hereafter referred to as RK), and made free use of standard results on Bessel functions (e.g., Jahnke and Emde [20]).

Our work is facilitated by use of two generic shifting operations:

Operation 1: $L^{-1}[g(s+i) - g(s-i)] = -2if(\tau)\sin\tau$, [RK, p. 170, Eq. (9)].
Operation 2: $L^{-1}[g(s+i) + g(s-i)] = 2f(\tau)\cos\tau$, [RK, p. 169, Eq. (8)].

where $f(\tau)$ and $g(s)$ denote a Laplace transform pair, that is, $f(\tau)$ is the original function and $g(s) = L[f(\tau)]$ is the corresponding image function.

Operation 1 applied to RK, p. 246, Eq. (14) yields:

$$L^{-1}\left[\exp(-\xi\sqrt{s+i}) - \exp(-\xi\sqrt{s-i})\right] = -i\frac{\xi\sin\tau}{\sqrt{\pi}\tau^{3/2}}\exp\left(-\frac{\xi^2}{4\tau}\right). \quad (A.1)$$

Operation 2 applied to RK, p. 246, Eq. (14) yields:

$$L^{-1}\left[\exp(-\xi\sqrt{s+i}) + \exp(-\xi\sqrt{s-i})\right] = \frac{\xi\cos\tau}{\sqrt{\pi}\tau^{3/2}}\exp\left(-\frac{\xi^2}{4\tau}\right). \quad (A.2)$$

Operation 1 applied to RK, p. 246, Eq. (15) yields:

$$L^{-1}\left[\sqrt{s+i}\exp(-\xi\sqrt{s+i}) - \sqrt{s-i}\exp(-\xi\sqrt{s-i})\right] = -i\frac{(\xi^2-2\tau)\sin\tau}{2\sqrt{\pi}\tau^{5/2}}\exp\left(-\frac{\xi^2}{4\tau}\right). \quad (A.3)$$

Operation 2 applied to RK, p. 246, Eq. (15) yields:

$$L^{-1}\left[\sqrt{s+i}\exp(-\xi\sqrt{s+i}) + \sqrt{s-i}\exp(-\xi\sqrt{s-i})\right] = \frac{(\xi^2-2\tau)\cos\tau}{2\sqrt{\pi}\tau^{5/2}}\exp\left(-\frac{\xi^2}{4\tau}\right). \quad (A.4)$$

Operation 1 applied to RK, p. 246, Eq. (18) yields:

$$L^{-1}\left[(s+i)\exp(-\xi\sqrt{s+i}) - (s-i)\exp(-\xi\sqrt{s-i})\right] = -i\xi\frac{(\xi^2-6\tau)\sin\tau}{4\sqrt{\pi}\tau^{7/2}}\exp\left(-\frac{\xi^2}{4\tau}\right). \quad (A.5)$$

Operation 2 applied to RK, p. 246, Eq. (18) yields:

$$L^{-1}\left[(s+i)\exp(-\xi\sqrt{s+i}) + (s-i)\exp(-\xi\sqrt{s-i})\right] = \xi\frac{(\xi^2-6\tau)\cos\tau}{4\sqrt{\pi}\tau^{7/2}}\exp\left(-\frac{\xi^2}{4\tau}\right). \quad (A.6)$$

RK, p. 207, Eq. (8) is

$$L^{-1}(\sqrt{s+i} - \sqrt{s-i}) = \frac{e^{i\tau} - e^{-i\tau}}{2\sqrt{\pi}\tau^{3/2}} = i\frac{\sin\tau}{\sqrt{\pi}\tau^{3/2}}. \quad (A.7)$$

RK, p. 209, Eq. (29) is $L^{-1}[(\sqrt{s+i} - \sqrt{s-i})^2] = i\frac{2I_1(i\tau)}{\tau}$, where I_1 is the modified Bessel function of the first kind of order one. This can be rewritten using

$I_1(i\tau) = iJ_1(\tau)$, where J_1 is the Bessel function of the first kind of order one:

$$L^{-1}\left[(\sqrt{s+i}-\sqrt{s-i})^2\right] = -\frac{2J_1(\tau)}{\tau}. \quad \text{(A.8)}$$

RK, p. 209, Eq. (29) is $L^{-1}[(\sqrt{s+i}-\sqrt{s-i})^3] = i^{3/2}\frac{3\sqrt{2}}{\tau}I_{3/2}(i\tau)$. This can be rewritten using $\sqrt{i}iI_{3/2}(i\tau) = -J_{3/2}(\tau)$, and the fact that Bessel functions of half-integer order can be expressed in closed form in terms of elementary functions. In the present case, $J_{3/2}(\tau) = \frac{\sqrt{2}}{\sqrt{\pi}\tau^{3/2}}(\sin\tau - \tau\cos\tau)$, and we obtain

$$L^{-1}\left[(\sqrt{s+i}-\sqrt{s-i})^3\right] = i\frac{6(\tau\cos\tau - \sin\tau)}{\sqrt{\pi}\tau^{5/2}}. \quad \text{(A.9)}$$

References

[1] B. Gebhart, Y. Jaluria, R.L. Mahajan, B. Sammakia, Buoyancy-Induced Flows and Transport, Hemisphere Publishing, New York, 1988 (Chapter7).

[2] C.R. Illingworth, Unsteady laminar flow of a gas near an infinite flat plate, Proc. Cambridge Philos. Soc. 46 (1950) 603–613.

[3] R. Siegel, Transient free convection from a vertical flat plate, Trans. ASME 80 (1958) 347–359.

[4] E.R. Menold, K.-T. Yang, Asymptotic solutions for unsteady laminar free convection on a vertical plate, Trans. ASME: J. Appl. Mech. 29 (1962) 124–126.

[5] J.A. Schetz, R. Eichhorn, Unsteady natural convection in the vicinity of a doubly-infinite vertical plate, Trans. ASME: J. Heat Transfer 84 (1962) 334–338.

[6] R.J. Goldstein, D.G. Briggs, Transient free convection about vertical plates and circular cylinders, Trans. ASME: J. Heat Transfer 86 (1964) 490–500.

[7] U.N. Das, R.K. Deka, V.M. Soundalgekar, Transient free convection flow past an infinite vertical plate with periodic temperature variation, J. Heat Transfer 121 (1999) 1091–1094.

[8] J.S. Park, J.M. Hyun, Transient behavior of vertical buoyancy layer in a stratified fluid, Int. J. Heat Mass Transfer 41 (1998) 4393–4397.

[9] J.S. Park, Transient buoyant flows of a stratified fluid in a vertical channel, KSME Int. J. 15 (2001) 656–664.

[10] A. Shapiro, E. Fedorovich, Unsteady convectively driven flow along a vertical plate immersed in a stably stratified fluid, J. Fluid Mech. 498 (2004) 333–352.

[11] A.E. Gill, The boundary layer regime for convection in a rectangular cavity, J. Fluid Mech. 26 (1966) 515–536.

[12] J.W. Elder, Laminar free convection in a vertical slot, J. Fluid Mech. 23 (1965) 77–98.

[13] A.E. Gill, A. Davey, Instabilities of a buoyancy-driven system, J. Fluid Mech. 35 (1969) 775–798.

[14] R.F. Bergholz, Instability of steady natural convection in a vertical fluid layer, J. Fluid Mech. 84 (1978) 743–768.

[15] Y. Joshi, B. Gebhart, Transition of vertical natural convection flows in water, J. Fluid Mech. 179 (1987) 407–438.

[16] A.M.H. Brooker, J.C. Patterson, T. Graham, W. Schöpf, Convective instability in a time-dependent buoyancy driven boundary layer, Int. J. Heat Mass Transfer 43 (2000) 297–310.

[17] J.C. Patterson, T. Graham, W. Schöpf, S.W. Armfield, Boundary layer development on a semi-infinite suddenly heated vertical plate, J. Fluid Mech. 453 (2002) 39–55.

[18] M. Van Dyke, Perturbation Methods in Fluid Mechanics, Parabolic Press, Stanford, 1975 (Chapter 2).

[19] G.E. Roberts, H. Kaufman, Table of Laplace Transforms, W.B. Saunders Co., Philadelphia, 1966.

[20] E. Jahnke, F. Emde, Tables of Functions, Dover Publications, New York, 1945 (Chapter 8).

[21] E. Fedorovich, F.T.M. Nieuwstadt, R. Kaiser, Numerical and laboratory study of a horizontally evolving convective boundary layer. Part I: Transition regimes and development of the mixed layer, J. Atmos. Sci. 58 (2001) 70–86.

[22] F.T.M. Nieuwstadt, Direct and large-eddy simulation of free convection. Proceedings of the Ninth International Heat Transfer Conference, Jerusalem, Israel, 1990, pp. 37–47.

[23] P.K. Kundu, I.M. Cohen, Fluid Mechanics, Second ed., Academic Press, San Diego, 2002, p. 708.